

# Eocene greenhouse climate revealed by coupled clumped isotope-Mg/Ca thermometry

David Evans<sup>1</sup>, Navjit Sagoo<sup>2</sup>, Willem Renema<sup>3</sup>, Laura Cotton<sup>4</sup>, Wolfgang Müller<sup>5</sup>, Jonathan Todd<sup>6</sup>, Pratul Saraswati<sup>7</sup>, Peter Stassen<sup>8</sup>, Martin Ziegler<sup>9</sup>, Paul Pearson<sup>10</sup>, Paul Valdes<sup>11</sup>, Hagit Affek<sup>12</sup>

<sup>1</sup>University of St Andrews, <sup>2</sup>Yale University, <sup>3</sup>Naturalis Biodiversity Center, <sup>4</sup>University of Florida, <sup>5</sup>Goethe University Frankfurt, <sup>6</sup>Natural History Museum, <sup>7</sup>Indian Institute of Technology Bombay, <sup>8</sup>KU Leuven, <sup>9</sup>Utrecht University, <sup>10</sup>Cardiff University, <sup>11</sup>University of Bristol, <sup>12</sup>Hebrew University of Jerusalem

Submitted to Proceedings of the National Academy of Sciences of the United States of America

Past greenhouse periods with elevated atmospheric CO<sub>2</sub> were characterized by globally warmer sea surface temperatures (SST). However, the extent to which the high-latitudes warmed to a greater degree than the tropics (polar amplification) remains poorly constrained, in particular because there are only a few temperature reconstructions from the tropics. Consequently, the relationship between increased CO<sub>2</sub>, the degree of tropical warming and the resulting latitudinal SST gradient is not well known. Here, we present coupled clumped isotope ( $\Delta_{47}$ )-Mg/Ca measurements of foraminifera from a set of globally distributed sites in the tropics and mid-latitudes.  $\Delta_{47}$  is insensitive to seawater chemistry and therefore provides a robust constraint on tropical SST. Crucially, coupling these data with Mg/Ca measurements allows the precise reconstruction of Mg/Ca<sub>sw</sub> throughout the Eocene, enabling the reinterpretation of all planktonic foraminifera Mg/Ca data. The combined dataset constrains the range in Eocene tropical SST to 30–36°C (from sites in all basins). We compare these accurate tropical SST to deep ocean temperatures, serving as a minimum constraint on high-latitude SST. This results in a robust conservative reconstruction of the early Eocene latitudinal gradient, which was reduced by at least 32±10% compared to present-day, demonstrating greater polar amplification than captured by most climate models.

clumped isotope | Eocene | tropical sea surface temperatures | polar amplification | seawater Mg/Ca

Greenhouse periods in the geological past have received much attention as indicators of the response of the Earth to elevated CO<sub>2</sub>. Of these, the Eocene is the most recent epoch characterized by pCO<sub>2</sub> at least twice pre-industrial, i.e. >560 ppm (1). Furthermore, as the quantity of paleoclimate reconstructions have increased the Eocene has become a target for comparison to climate models (2), as proxy data of past warm periods are required to assess model competence at elevated CO<sub>2</sub> (3). Existing geochemical proxy data suggest that the Eocene latitudinal SST gradient was greatly reduced: the mid-high latitude (>40°) surface oceans were 10–25°C warmer than today throughout the Eocene (4, 5), yet there is no evidence for tropical SST warming of a similar magnitude, even during peak warm intervals such as the Paleocene-Eocene Thermal Maximum (PETM) (6, 7). In fact, several studies have reported moderate tropical warmth (30–34°C) throughout the Eocene (8, 9). This is in contrast to most Eocene climate model simulations (10, 11), which indicate the latitudinal gradient was within 20% of modern (with notable exceptions (12), discussed below). However, using proxies to validate model output is problematic because many paleothermometers are associated with relatively large (often systematic) errors and are sensitive to diagenetic alteration after burial in sediment. For example, initial reconstructions of the Eocene tropics were biased by the analysis of poorly-preserved material, resulting in the cool-tropics hypothesis (13). Subsequently, it was shown that well-preserved samples yield Eocene tropical SST at least as warm as present (14–16). Furthermore, carbonate-bound proxies such as foraminiferal  $\delta^{18}\text{O}$  and Mg/Ca are highly

sensitive to poorly-constrained secular variations in salinity and seawater chemistry (17), TEX<sub>86</sub> is associated with calibration complications (18, 19), and all proxies may be seasonally biased to summer temperatures at mid-high latitudes (20). As a result, absolute tropical SST are not constrained to better than  $\pm\sim 5^\circ\text{C}$  at any given site (21), in part derived from uncertainties over whether modern calibrations are applicable to Eocene material (20). Similarly, atmospheric processes, in particular clouds and aerosol-cloud interactions are a large source of uncertainty within climate models (22), whilst variable inter-model sensitivities to CO<sub>2</sub> (10) complicate the use of these to directly constrain absolute Eocene temperatures. Given these uncertainties in both the data and models, there is no consensus regarding the degree of polar amplification or the precise response of the tropical oceans to increasing CO<sub>2</sub>. Specifically, much debate has focused on whether the tropics underwent substantial warming and the latitudinal gradient was only moderately reduced (23, 24), or if tropical warmth was limited and the gradient was far lower than today (9, 25). Hence, improved reconstructions, especially in the tropics, are of fundamental importance in understanding both the response of SST to increased CO<sub>2</sub> as well as the accuracy of climate models. We address these issues through coupled clumped isotope-Mg/Ca measurements of shallow-dwelling large benthic foraminifera (LBF) of the family Nummulitidae. Our fossil samples come from seven globally-distributed sites, four of which are in the tropics, including the equatorial West Pacific/Indian Ocean (Fig. 1). In order to expand this dataset to produce a global picture of Eocene tropical climate, we also produce a precise Eocene seawater Mg/Ca curve and use it to reinterpret all published Mg/Ca data from an additional 12 sites.

## Significance

Reconstructing the degree of warming during geological periods of elevated CO<sub>2</sub> provides a way of testing our understanding of the Earth system and the accuracy of climate models. We present accurate estimates of tropical sea surface temperatures (SST) and seawater chemistry during the Eocene (56–34 million years before present, CO<sub>2</sub> >560 ppm). This latter dataset enables us to reinterpret a large amount of existing proxy data. We find that tropical SST are characterized by a modest warming in response to CO<sub>2</sub>. Coupling these data to a conservative estimate of high-latitude warming demonstrates that most climate simulations do not capture the degree of Eocene polar amplification.

## Reserved for Publication Footnotes

137  
138  
139  
140  
141  
142  
143  
144  
145  
146  
147  
148  
149  
150  
151  
152  
153  
154  
155  
156  
157  
158  
159  
160  
161  
162  
163  
164  
165  
166  
167  
168  
169  
170  
171  
172  
173  
174  
175  
176  
177  
178  
179  
180  
181  
182  
183  
184  
185  
186  
187  
188  
189  
190  
191  
192  
193  
194  
195  
196  
197  
198  
199  
200  
201  
202  
203  
204

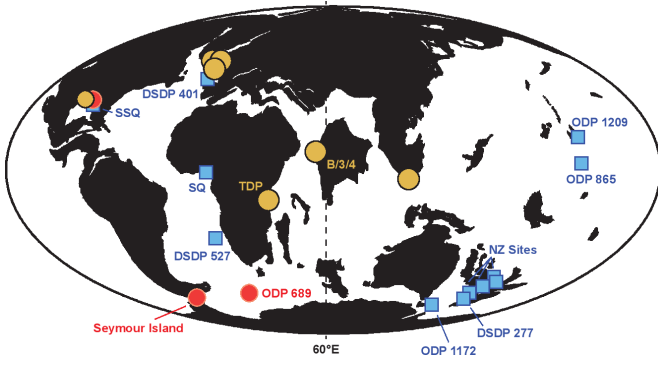


**Fig. 1.** Sample sites overlain on early Eocene paleogeography (created using <http://www.ods.de/ods/services/paleomap/paleomap.html>, after ref. (52)). Yellow circles - this study ( $\Delta_{47}$  and Mg/Ca), red circles - previous  $\Delta_{47}$  reconstructions, blue squares - published Eocene Mg/Ca data reinterpreted here using the seawater Mg/Ca reconstruction of this study. Sites without labels are terrestrial outcrops (see SI Appendix, Tab. S2).

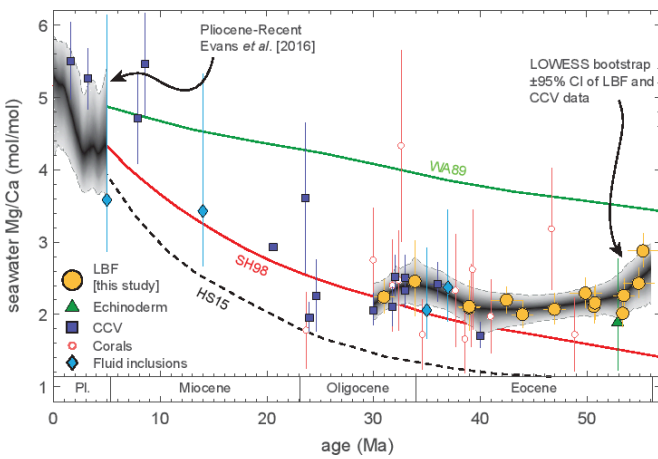


**Fig. 2.** Seawater Mg/Ca reconstruction for the Eocene and early Oligocene based on coupled  $\Delta_{47}$ -Mg/Ca Large Benthic Foraminifera (LBF) data, shown in the context of previous Cenozoic reconstructions (33, 34, 53, 54) and box-models (35, 36, 55; WA89, SH98 and HS15 respectively), that are commonly used for calculating planktonic and deep benthic foraminifera Mg/Ca data. CCV - ridge-flank  $\text{CaCO}_3$  veins. Coral-derived data younger than 20 Ma are omitted. The 95% confidence intervals on our Eocene Mg/Ca<sub>sw</sub> curve are derived from bootstrapping 1000 LOWESS fits, including both geochemical and dating uncertainties.

**Eocene surface ocean temperature from foraminifera clumped isotopes**

The carbonate clumped isotope thermometer (26, 27), hereafter denoted  $\Delta_{47}$ , is based on the increasingly preferential binding of heavy isotopes to each other (e.g.  $^{13}\text{C}$ - $^{18}\text{O}$  in carbonate) at lower temperatures. The principal advantage over existing geochemical temperature proxies is that there is no resolvable dependence on seawater elemental or isotopic composition (28), and uncertainty is dominated by analytical noise so that, unlike other carbonate-bound proxies, paleotemperature errors are random rather than systematic.

The epifaunal foraminifera utilized here live at approximately the same depth as planktonic species considered to be surface dwelling (29) (<50 m, within  $1^\circ\text{C}$  of SST in the tropics; see SI Appendix, Fig. S6), and calcify at a constant rate in locations characterized by a large seasonal cycle (30). Therefore, our paleotemperatures reflect mean annual SST. The abundance of the nummulitids in the Eocene tropics and mid-latitudes, where they are rock-forming in some locations, demonstrates that they

were well-adapted to the climate at the time. Three LBF species live-collected from seven locations are characterized by a  $\Delta_{47}$ -temperature slope within error of the Yale inorganic calcite calibration (27) (see SI Appendix, Fig. S1, Tab. S1), and there is no evidence for a significant vital effect influence on shell  $\delta^{18}\text{O}$ . These observations provide the basis for the use of this calibration to reconstruct paleotemperatures from extinct LBF of the same family.

All fossil samples were analyzed by laser-ablation ICPMS for a suite of trace elements to assess their geochemical preservation, together with SEM images (see SI Appendix, Fig. S4, Tab. S3). Trace element ratios indicative of contamination and overgrowths (Al/Ca and Mn/Ca) show no correlation with Mg/Ca, indicating the absence of any Mg-bearing secondary phase. SEM images of broken specimens show that Eocene and modern foraminifera are characterized by equivalent chamber wall micro-textures, demonstrating the absence of micron-scale recrystallisation. Furthermore, high-Mg calcite, such as that of LBF shells, recrystallizes fully to low-Mg, low-Sr calcite during diagenesis (see SI Appendix, Fig. S5), enabling the unambiguous identification of geochemically well-preserved material. On the basis of these screening techniques, only samples that were exceptionally well-preserved were utilized for  $\Delta_{47}$  analysis, i.e. those with no discernable diagenetic modification. Finally, because these foraminifera live at shallow water depths, there is no potential for a large difference between calcification and diagenetic temperature, unlike tropical planktonic species (15).

The mean tropical SST derived from samples that passed this rigorous screening is  $32.5 \pm 2.5^\circ\text{C}$  (Fig. 3A). The maximum reconstructed Eocene  $\Delta_{47}$  temperature is  $36.3 \pm 1.9^\circ\text{C}$  from Java at  $\sim 39$  Ma (all uncertainties are 1SE), with a paleolatitude of  $6^\circ\text{S}$  (30), possibly placing it within an expanded Indo-Pacific warm pool. Samples spanning the early Eocene (55.3-49.9 Ma) from Kutch, India, which was within  $5^\circ$  of the equator at that time, are characterized by temperatures of  $30.4 \pm 2.5$  to  $35.1 \pm 2.6^\circ\text{C}$ . The difficulty in precisely temporally correlating shallow sites means that we cannot definitively assign these samples to specific intervals, although the youngest and warmest Kutch sample probably falls within the Early Eocene Climatic Optimum (EECO;  $\sim 52$ -50 Ma). Although the peak temperature from equatorial India in the early Eocene is marginally cooler than that from middle Eocene Java, the two are within error, and this small difference may be explained by regionally cooler SST on the West coast of India compared to the West Pacific. A latest Eocene sample from Tanzania (33.9 Ma;  $21^\circ\text{S}$ ) records  $29.7 \pm 3.1^\circ\text{C}$ .

In addition, samples spanning the early-middle Eocene from northwest Europe were analyzed for  $\Delta_{47}$ - and Mg/Ca. The principal aim of doing so was to fill temporal gaps in our seawater chemistry reconstructions (see below), but these also provide new Eocene SST for this region. We observe a  $9^\circ\text{C}$  warming between the earliest Eocene ( $18$ - $20^\circ\text{C}$ ) and the EECO ( $28$ - $31^\circ\text{C}$ ), followed by a long-term cooling trend through the mid-Eocene to  $23.1 \pm 2.5^\circ\text{C}$  at 42.5 Ma. This pattern of global change is in good agreement with mid-high latitude TEX<sub>86</sub> (see SI Appendix, Fig. S8 and (31)).

Finally, calculated  $\delta^{18}\text{O}_{\text{sw}}$ , derived from  $\delta^{18}\text{O}_{\text{c}}$  measured simultaneously with  $\Delta_{47}$ , yield values that are in agreement with an ice-free world. Specifically,  $\delta^{18}\text{O}_{\text{sw}}$  reconstructed from our tropical samples is within error of  $-1\text{‰}$ , with the exception of Tanzania ( $-0.2\text{‰}$ ).  $\delta^{18}\text{O}_{\text{sw}}$  at our mid-latitude sites is temporally variable and characterized by overall more negative values, consistent with mid-latitude freshwater contribution to these proximal sites ( $-4$  to  $-1.5\text{‰}$ ). These data further demonstrate that our samples are well-preserved, and that the sample site salinity was not substantially lower than open ocean (all  $\delta^{18}\text{O}_{\text{sw}}$  within  $3\text{‰}$  of mean Eocene seawater). Because a  $>10$  psu salinity reduction is necessary to significantly change seawater Mg/Ca (Mg/Ca<sub>sw</sub>),

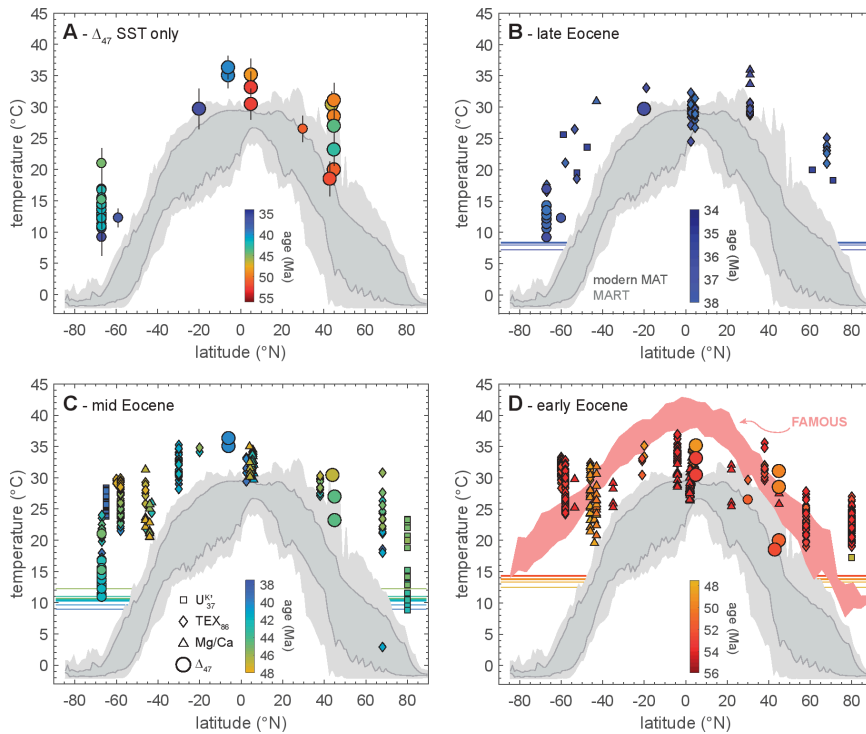


**Fig. 3.** Eocene clumped isotope SST reconstruction and re-evaluated Mg/Ca temperatures (this study) shown in the context of organic proxies. (A) All clumped isotope-derived SST. Smaller symbols are previously published data. (B-D) Absolute Eocene SST proxy data, split into three time intervals (34-38, 38-48 and 48-56 Ma). All Mg/Ca data were reevaluated based on our Mg/Ca<sub>sw</sub> curve (Fig. 2). TEX<sub>86</sub> temperatures were recalculated using the TEX<sub>86</sub><sup>H</sup> calibration (56). See SI Appendix for references. Horizontal lines show Eocene Mg/Ca-derived deep ocean temperatures (44). The modern mean annual temperature (MAT) and seasonal range in SST (MART) are depicted by dark and light grey shading, respectively. Marker and line color depicts sample age, note the colour scale is the same in all panels. Data are compared to an Eocene GCM simulation (FAMOUS model E17 (46) at 560 ppm CO<sub>2</sub>) in panel D.

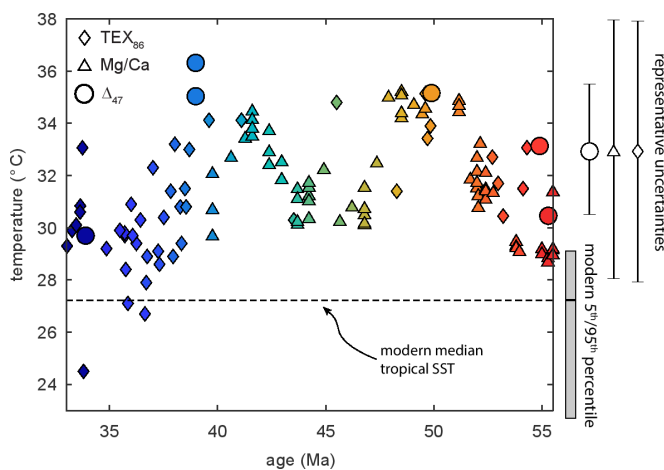


**Fig. 4.** The evolution of tropical (<23°) sea surface temperatures through the Eocene. Note that scatter in the proxy data is of a similar magnitude as the modern range in tropical SST (grey bar). Representative errors are 1SE for Δ<sub>47</sub>, propagated uncertainties derived from the influence of Mg/Ca<sub>sw</sub> and pH on Mg/Ca, and 2SE for TEX<sub>86</sub>. The modern mean and 95<sup>th</sup> percentiles are based on the World Ocean Atlas (see the SI Appendix).

our LBF Mg/Ca data discussed below must also represent normal seawater conditions (see SI Appendix, Fig. S7).

Our samples do not include the PETM, and only one falls within the EECO. Therefore, our results do not preclude warmer tropical temperatures during those time intervals (6). Nonetheless, we find no evidence for tropical SST >38°C based on our Δ<sub>47</sub> data. Indeed, all of our tropical data are within uncertainty of each other, and could be interpreted as indicating stable warm conditions in the tropics throughout the Eocene (32.5±2.5°C), in line with several previous studies (8, 14, 32), although possible temporal trends will be discussed below. To assess whether a similar picture is evident in other proxy SST data, and therefore to address the broader questions of the Eocene evolution of

tropical SST and early Eocene polar amplification, we use these Δ<sub>47</sub> paleotemperatures, together with Mg/Ca analyses of the same samples, to accurately and precisely reconstruct seawater Mg/Ca (Mg/Ca<sub>sw</sub>). This allows us to reevaluate all Eocene planktonic foraminifera Mg/Ca data, providing an additional constraint on tropical SST at higher temporal and spatial resolution than the Δ<sub>47</sub> data alone. Furthermore, by combining information from these proxies we create a large dataset consisting mostly of open ocean data, suitable for comparison to climate simulations. Doing so minimizes potential bias associated with the regional paleoceanography of any individual site.

### Seawater Mg/Ca reconstruction

Coupling Mg/Ca-Δ<sub>47</sub> data of the same specimens allows us to simultaneously reconstruct temperature and Mg/Ca<sub>sw</sub> because shell Mg/Ca is a function of both, and we independently constrain the temperature component of Mg incorporation using Δ<sub>47</sub>. Although much work has focused on reconstructing past variation in Mg/Ca<sub>sw</sub> (33, 34), a different approach is required. Whilst these studies show that Mg/Ca<sub>sw</sub> has approximately doubled since the Oligocene (35), precise reconstructions for most of the Paleogene are lacking, and models covering the Phanerozoic (35, 36) do not agree on epoch-scale variation in seawater chemistry. This has precluded reliable Mg/Ca-derived paleotemperatures with sufficient accuracy for assessing model SST competency (17). To overcome this, we use Δ<sub>47</sub> data of LBF spanning the Eocene-early Oligocene to solve the Mg/Ca<sub>LBF</sub>-Mg/Ca<sub>sw</sub>-temperature calibration for these foraminifera (37). The uncertainty in these reconstructions is ~2-5 times lower than previous estimates, reducing the Mg/Ca<sub>sw</sub>-derived error on existing planktonic foraminifera temperatures to <2.5°C. This is possible because nummulitid Mg/Ca is more sensitive to Mg/Ca<sub>sw</sub> than to temperature, and unlike planktonic species there are no resolvable salinity or carbonate chemistry effects (30, 37). The composite Paleogene Mg/Ca<sub>sw</sub> curve (Fig. 2) is based on our LBF and data from inorganic vein carbonates (33), as the uncertainty on these latter data is also relatively small and the two records are in excellent agreement where they overlap. This reconstruction delineates the



409  
410  
411  
412  
413  
414  
415  
416  
417  
418  
419  
420  
421  
422  
423  
424  
425  
426  
427  
428  
429  
430  
431  
432  
433  
434  
435  
436  
437  
438  
439  
440  
441  
442  
443  
444  
445  
446  
447  
448  
449  
450  
451  
452  
453  
454  
455  
456  
457  
458  
459  
460  
461  
462  
463  
464  
465  
466  
467  
468  
469  
470  
471  
472  
473  
474  
475  
476

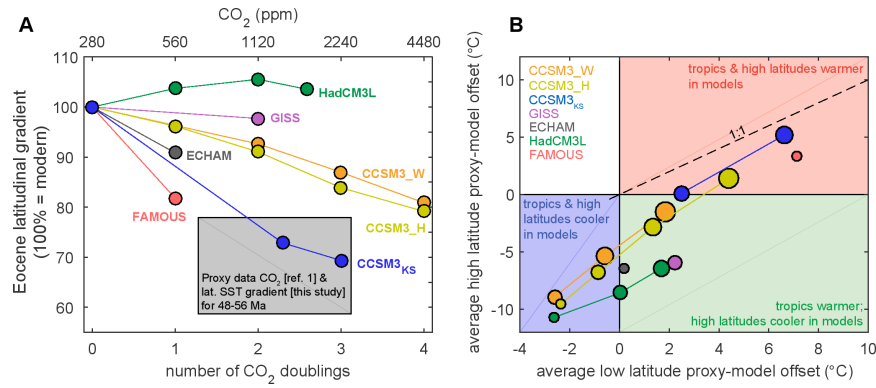


**Fig. 5.** Early Eocene (48-56 Ma) model-data comparison. **(A)** Zonally-averaged latitudinal gradients based on proxy CO<sub>2</sub> and SST data (grey box) and climate models (12, 46-48, 50, 57) (circles) over a range of CO<sub>2</sub>. Proxy CO<sub>2</sub> range is from (1) including error, the gradient uncertainty is the combined 2SE of the tropical and high latitude proxy data (see text). Proxy-derived gradient is shown relative to present day, Eocene climate model simulations are shown relative to their pre-industrial counterpart. Most model simulations do not capture the reduced latitudinal gradient within the range of proxy CO<sub>2</sub> (<2250 ppm). **(B)** Site specific model-data comparison for the tropics and high latitudes. Model SST competency assessed by comparing the mean difference between the model and proxy data for low and high-latitudes. Quadrants reflect different overall patterns of model-data offset. Hypothetical simulations falling on the 1:1 line would reconstruct the same latitudinal gradient as the data but not the same absolute SST, except at the origin. All models fall below this line, indicating that Eocene polar amplification is underestimated.

Eocene-early Oligocene as a period of stable Mg/Ca<sub>sw</sub> between 2.1-2.5 mol mol<sup>-1</sup>, ~45% of modern. Previously, the lack of data before 40 Ma required box-model estimates (35, 36) to be used to assess the impact of secular change in seawater chemistry on fossil Mg/Ca measurements. The precise LBF-derived Mg/Ca<sub>sw</sub> data (Fig. 2) demonstrate that those models are inaccurate in the early Eocene, with a large effect on Mg/Ca-derived temperatures. For example, early Eocene tropical SST calculated using our Mg/Ca<sub>sw</sub> would result in temperatures 6-10°C cooler compared to the model output of ref. (35), yet warmer by a similar magnitude using the model of ref. (36).

### Eocene tropical warmth

In light of both our tropical clumped isotope data and revised planktonic foraminifera Mg/Ca temperatures utilizing the precise Mg/Ca<sub>sw</sub> reconstruction described above, we are able to estimate low-latitude SST across the globe and throughout the Eocene, thus placing new constraints on the early-Eocene latitudinal gradient (Fig. 3,4). When doing so it must be considered that in addition to Mg/Ca<sub>sw</sub>, both salinity and the carbonate system may bias planktonic foraminifera Mg/Ca-derived SST (21, 38). We consider the impact of pH in detail (see SI Appendix), but do not apply a salinity correction because mean Eocene ocean salinity was similar to today (39). Although Mg/Ca and TEX<sub>86</sub> are associated with relatively large uncertainties (~±3-5°C) related to non-thermal influences and calibration complications, Δ<sub>47</sub>, reinterpreted planktonic Mg/Ca, and TEX<sub>86</sub> are in good agreement in the tropics. This indicates that if either of the latter are systematically offset in this region, it is by less than the magnitude of the stated error, lending support to the interpretation of Eocene GDGTs in terms of SST in the tropics (cf. ref. (19, 40)).

The tropical compilation constrains SST to between 30-36°C throughout the Eocene (Fig. 4), with the exception of late Eocene TEX<sub>86</sub> from ODP Site 929/925 (31) which range between 27-32°C, and the earliest Eocene Mg/Ca data from ODP Site 865 (26-31°C). Although the Δ<sub>47</sub> reconstructions from the middle Eocene of Java are 1°C higher than the EECO of Kutch this may simply reflect zonal differences in Eocene tropical SST, which is likely given that the modern tropics are characterized by similar zonal SST variability (Fig. 4). Additionally, the compilation highlights that the 2-5°C tropical warming between the earliest Eocene and the EECO shown by the Δ<sub>47</sub> data from Kutch is in good agreement with planktonic foraminifera Mg/Ca from ODP Site 865 (recalculated from ref. (41)) and earliest Eocene TEX<sub>86</sub> data

(6); early Eocene equatorial clumped isotope temperatures of 30-33°C are therefore not anomalously cool.

These data do not rule out the possibility of higher temperatures over transient events such as the PETM (6), and therefore do not constrain peak Eocene tropical warmth. They do provide strong evidence that the early Eocene tropical oceans in general were not warmer than 36°C (mean ~33°C, upper uncertainty 38°C), unless all proxies are biased towards lower temperatures. Given that there is no reason to suspect this, our data provide a well-constrained basis to examine the early Eocene latitudinal gradient and the accuracy of Eocene model simulations.

### Early Eocene latitudinal sea surface temperature gradient

To use our tropical SST compilation to quantitatively constrain the equator-pole SST gradient for the early Eocene (the interval to which most model simulations are compared), we first review the high-latitude proxy data. Eocene SSTs derived from TEX<sub>86</sub> data from the ACEX core (42) (~80°N), ODP Site 1172 (5) (~54°S) and Wilkes Land (43) (~60°S) greatly exceed deep ocean temperatures derived from deep benthic foraminifera Mg/Ca and δ<sup>18</sup>O (44), suggesting either a seasonal bias, the influence of local warm surface currents, a more stratified ocean, and/or uncertain calibrations (20). To avoid these complications, we use the deep-benthic foraminifera-Mg/Ca temperature stack (44) as a lower limit on high-latitude SST. Present-day mean SST at high-latitudes is within 1°C of the deep ocean (see the SI Appendix), and the coolest Eocene high-latitude Δ<sub>47</sub> data based on long-lived shallow benthic molluscs from Seymour Island (45) are within error of coeval deep-ocean temperatures where both are available (Fig. 3B,C). Although the coherence of these reconstructions supports the use of deep ocean Mg/Ca as a minimum constraint on high-latitude SST through time, model evidence suggest that Eocene deep water formation in the Southern Ocean may have been limited to winter (20), resulting in colder deep water compared to mean annual high-latitude SST. Therefore, we emphasize that using the benthic foraminifera Mg/Ca dataset as a proxy for the high-latitude SST produces an estimate of the *maximum* steepness of the latitudinal SST gradient and does not necessarily represent the mean annual gradient. Similarly, it does not in itself provide a means of assessing high-latitude SST proxy data given that these may be biased towards a different season, and there is evidence for a zonal SST heterogeneity in the Eocene Southern Ocean (45). The merit in this approach is that it provides a conservative constraint on the degree to which the

477  
478  
479  
480  
481  
482  
483  
484  
485  
486  
487  
488  
489  
490  
491  
492  
493  
494  
495  
496  
497  
498  
499  
500  
501  
502  
503  
504  
505  
506  
507  
508  
509  
510  
511  
512  
513  
514  
515  
516  
517  
518  
519  
520  
521  
522  
523  
524  
525  
526  
527  
528  
529  
530  
531  
532  
533  
534  
535  
536  
537  
538  
539  
540  
541  
542  
543  
544

545 gradient was reduced in the Eocene, and therefore represents the  
546 minimum that model simulations must achieve in order to be con-  
547 sidered representative of Eocene climate. We calculate the early  
548 Eocene latitudinal gradient as the difference between the mean  
549 tropical and deep-ocean data between 48-56 Ma ( $\pm 2$ SE variability  
550 in both datasets); it is therefore representative of background  
551 early Eocene conditions (i.e. not the PETM, for which there is  
552 evidence for a further reduction in the latitudinal SST gradient  
553 (21)).

554 Based on this analysis, we find a reduction of at least  $32\pm 10\%$   
555 in the mean difference between tropical and high-latitude SST  
556 during the early Eocene (48-56 Ma), relative to present-day (Fig.  
557 5A). The quantity ( $n = 123$ ) and coherence of tropical early  
558 Eocene data from  $\Delta_{47}$  and two other proxies means that we can  
559 confidently use this as a conservative estimate to assess model  
560 competency. Splitting the early Eocene into intervals approximat-  
561 ing the EECO (50-52.5 Ma) versus post-PETM, pre-EECO (55-  
562 52.5 Ma) does not significantly alter our finding as the latitudinal  
563 gradient for both intervals is within the uncertainty of the early  
564 Eocene data overall. Therefore, for the purposes of model-data  
565 comparison we do not split the early Eocene in this way because  
566 the overall sparsity of data may result in a regionally biased  
567 comparison.

### 568 Eocene model-data comparison

569 Polar amplification in climate models of past warm periods  
570 has received much attention as it has long been suggested that  
571 simulations may not capture the extent to which the latitudinal  
572 SST gradient is reduced. In the Eocene, this debate has focused  
573 in part on the magnitude of tropical warming (23). For example,  
574 if tropical SST were far higher than at present and if high-  
575 latitude proxy data were summer-biased, then some models are  
576 in overall agreement with the data (20). Our  $\Delta_{47}$  reconstructions  
577 and SST compilation (Fig. 3,4) demonstrate that early Eocene  
578 tropical warming was of a substantially lower magnitude than  
579 in most models, and therefore indicate that the proxy data are  
580 irreconcilable with these simulations even when accounting for  
581 complicating factors in the high-latitudes. Other simulations in-  
582 dicate SST exceeding the proxy estimates in both the tropics  
583 and high-latitudes. For example, the FAMOUS model simulation  
584 (46) shown in the context of the early Eocene proxy data in  
585 Fig. 3D is notable because it produces a substantially reduced  
586 latitudinal SST gradient. However, the parameter changes used  
587 to achieve this gradient reduction result in tropical SST that are  
588  $\sim 7^\circ\text{C}$  warmer than the proxy data.

589 Extending this comparison (Fig. 5A) by comparing the  
590 Eocene data latitudinal gradient to a number of climate simula-  
591 tions shows that HadCM3L (47) and GISS (48) are characterized  
592 by SST gradients within 10% of their pre-industrial simulation.  
593 In contrast, CCSM (as configured by refs. (49, 50)) approaches  
594 the proxy gradient at four  $\text{CO}_2$  doublings (4480 ppm), whilst the  
595 CCSM models of ref. (12) (hereafter CCSM<sub>KS</sub>) and the warmest  
596 FAMOUS simulation (46) fall within the range of the proxy data,  
597 achieving latitudinal gradients below 80% of modern at 560 ppm  
598  $\text{CO}_2$ . The common feature of these latter models is that both have  
599 substantially modified parameters related to cloud formation  
600 including a reduction in low-level stratiform cloud, increased pre-  
601 cipitation rates, and an increase in incoming shortwave radiation.  
602 Such clouds are more prevalent at high-latitudes, resulting in  
603 preferential surface warming of these regions.

604 Although models with modified cloud properties are within  
605 error of a conservative latitudinal proxy gradient, this does not  
606 imply agreement in terms of absolute temperatures (e.g. compare  
607 FAMOUS to the data in Fig. 3D). Therefore, to assess the ability  
608 of models to reconstruct both absolute SST and the latitudinal  
609 gradient, and to avoid the potential bias introduced  
610 by condensing model-data comparison into a latitudinal transect,  
611 the offsets between the proxy data and the nearest model grid

612 cells were calculated to produce a location-specific proxy-model  
613 comparison. Fig. 5B and S12-14 display the result of this exercise  
614 in terms of the average tropical and high-latitude proxy-model  
615 offset, i.e. the mean of location-specific offsets between the model  
616 and data for the two regions (as above, the high-latitude proxy-  
617 model offset was conservatively estimated based on deep ocean  
618 temperatures, see SI Appendix). Models with Eocene latitudi-  
619 nal gradients similar to present-day such as HadCM3L and  
620 ECHAM (Fig. 5A) consistently underestimate high-latitude SST.  
621 Moreover, we find that no simulation captures our conservative  
622 estimate of the latitudinal gradient and the absolute proxy tem-  
623 peratures. Specifically, most models that lie close to the 1:1 line  
624 in Fig. 5B, representing agreement in terms of the latitudinal  
625 gradient, overestimate both tropical and high-latitude SST and  
626 require  $p\text{CO}_2$  greater than that indicated by the proxy data.  
627 Nonetheless, three CCSM simulations fall within 2-3°C of the  
628 origin in Fig. 5B, indicating that these are close to reproducing our  
629 conservative analysis of the early Eocene latitudinal gradient, as  
630 well as the absolute proxy temperatures. CCSM<sub>KS</sub>, with modified  
631 cloud properties, achieves this with  $p\text{CO}_2$  within the range of  
632 proxy data (1). However, we stress that our derivation of the  
633 early Eocene latitudinal gradient is conservative. If high-latitude  
634 mean annual SST were in fact warmer than the deep ocean, then  
635 the model-data comparison would be considerably less favorable.  
636 Similarly, evidence for further polar amplification during the  
637 PETM (21) predicts a less-favorable comparison. Therefore, our  
638 analysis indicates that a further mechanism of polar amplification  
639 is likely to be required to fully reconcile models with peak Eocene  
640 warmth, given that CCSM<sub>KS</sub> (the best performing model in our  
641 analysis) is characterized by a similar latitudinal SST gradient  
642 when run under pre-PETM and PETM conditions (Fig. 5A).

643 Our coupled  $\Delta_{47}$ -Mg/Ca data and subsequent reanalysis of  
644 planktonic Mg/Ca temperatures via the precise reconstruction of  
645  $\text{Mg}/\text{Ca}_{\text{sw}}$  demonstrate that the early Eocene mean latitudinal SST  
646 gradient was at least  $32\pm 10\%$  shallower than modern. Based on  
647 a location-specific comparison that avoids latitudinal averaging,  
648 we find that few modelling efforts (12) are close to reproducing  
649 both this gradient and the absolute proxy SST. Further work  
650 is required to capture the possible additional reduction in this  
651 gradient during peak warm intervals, or if Eocene mean annual  
652 high-latitude SST were warmer than the deep ocean. The most  
653 accurate Eocene simulations with respect to SST independently  
654 achieved this by modifying aerosol and cloud properties, high-  
655 lighting the importance of this research direction as a potential  
656 mechanism for polar amplification (51).

### 657 Materials and Methods

658 All fossil samples come from clay or sand horizons (e.g. ref. (30)) and none  
659 contained noticeable carbonate inclusions that may bias the data. Addition-  
660 ally, broken chamber wall sections of key samples were imaged by SEM in  
661 order to confirm that  $\mu\text{m}$ -scale recrystallization had not taken place.

662 Samples were analyzed by laser-ablation ICPMS using the RESolution  
663 M-50 system at Royal Holloway University of London (58). The procedure  
664 for non-destructive analysis of LBF has been described in detail elsewhere  
665 (37), and was modified only in that the Agilent 7500 ICPMS used in that  
666 study was replaced with an Agilent 8800 triple-quadrupole ICPMS part-way  
667 through the analytical period. Prior to clumped isotope measurement every  
668 specimen was analyzed by LA-ICPMS to assess preservation on an individual  
669 specimen basis. The only exception to this was sample W10-3c and EF1/2,  
670 which contained abundant foraminifera, and all specimens analyzed were  
671 found to be geochemically well-preserved. Therefore, screening of every  
672 foraminifera was unnecessary. Aside from widely used preservation indica-  
673 tors such as Al/Ca for clay contamination and Mn/Ca for overgrowths, Mg/Ca  
674 and Sr/Ca are also useful preservation indicators as the Mg and Sr concen-  
675 tration of high-Mg calcite decreases substantially upon recrystallization to  
676 values substantially lower than well-preserved Eocene specimens (pervasively  
677 recrystallized samples are shown for comparison, see SI Appendix, Fig. S5).

678 The clumped isotope analytical procedure at Yale University is described  
679 in detail elsewhere (45, 59). Larger specimens were crushed before cleaning,  
680 smaller specimens were analyzed as multiple whole shells. Modern samples  
681 were ultrasonicated for 30 minutes in  $\sim 7\%$   $\text{H}_2\text{O}_2$ , rinsed three times  
682 in distilled water and dried under vacuum at  $25^\circ\text{C}$ . Fossil samples with lower  
683 organic content were ultrasonicated in methanol followed by distilled water

681  
682  
683  
684  
685  
686  
687  
688  
689  
690  
691  
692  
693  
694  
695  
696  
697  
698  
699  
700  
701  
702  
703  
704  
705  
706  
707  
708  
709  
710  
711  
712  
713  
714  
715  
716  
717  
718  
719  
720  
721  
722  
723  
724  
725  
726  
727  
728  
729  
730  
731  
732  
733  
734  
735  
736  
737  
738  
739  
740  
741  
742  
743  
744  
745  
746  
747  
748

only to remove any clay adherents. Then ~3-5 mg of sample was reacted overnight with 103-105% H<sub>3</sub>PO<sub>4</sub> at 25°C. The CO<sub>2</sub> was extracted through an H<sub>2</sub>O trap and cleaned of volatile organic compounds using a 30 m Supelco Q-Plot GC column at -20°C. Isotopic analyses were performed on a Thermo MAT253 optimized to measure m/z 44-49. Masses 48 and 49 were used to assess sample purity. Standardization was performed through the analysis of CO<sub>2</sub> with a range of δ<sup>18</sup>O and δ<sup>13</sup>C, heated to 1000°C (termed 'heated gases') and transferred into the absolute reference frame as previously described (59, 60) using standards with a Δ<sub>47</sub> range that spans the samples (see SI Appendix for details).

1. Anagnostou E, et al. (2016) Changing atmospheric CO<sub>2</sub> concentration was the primary driver of early Cenozoic climate. *Nature* 533(7603):380–384.
2. Lunt DJ, et al. (2017) The DeepMIP contribution to PMIP4: Experimental design for model simulations of the EECO, PETM, and pre-PETM (version 1.0). *Geosci Model Dev* 10(2):889–901.
3. Haywood AM, et al. (2011) Are there pre-Quaternary geological analogues for a future greenhouse warming? *Philos Trans A Math Phys Eng Sci* 369(1938):933–56.
4. Hollis CJ, et al. (2009) Tropical sea temperatures in the high-latitude South Pacific during the Eocene. *Geology* 37(2):99–102.
5. Bijl PK, et al. (2009) Early Palaeogene temperature evolution of the southwest Pacific Ocean. *Nature* 461(7265):776–9.
6. Frieling J, et al. (2017) Extreme warmth and heat-stressed plankton in the tropics during the Paleocene-Eocene Thermal Maximum. *Geology* (8):e1600891.
7. Aze T, et al. (2014) Extreme warming of tropical waters during the Paleocene-Eocene thermal maximum. *Geology* 42(9):739–742.
8. Pearson PN, et al. (2007) Stable warm tropical climate through the Eocene Epoch. *Geology* 35(3):211.
9. Keating-Bitonti CR, Ivany LC, Affek HP, Douglas P, Samson SD (2011) Warm, not super-hot, temperatures in the early Eocene subtropics. *Geology* (8):771–774.
10. Lunt DJ, et al. (2012) A model–data comparison for a multi-model ensemble of early Eocene atmosphere–ocean simulations: EoMIP. *Clim Past* 8(5):1717–1736.
11. Lunt DJ, et al. (2013) Warm climates of the past—a lesson for the future? *Philos Trans R Soc A Math Phys Eng Sci* 371(2001):20130146–20130146.
12. Kiehl JT, Shields C a (2013) Sensitivity of the Paleocene-Eocene Thermal Maximum climate to cloud properties. *Philos Trans A Math Phys Eng Sci* 371(2001):20130093.
13. Shackleton NJ, Boersma A (1981) The climate of the Eocene ocean. *J Geol Soc London* 138:153–157.
14. Pearson PN, et al. (2001) Warm tropical sea surface temperatures in the Late Cretaceous and Eocene epochs. *Nature* 413(6855):481–7.
15. Schrag DP, Depaolo DJ, Richter FM (1995) Reconstructing past sea surface temperatures : Correcting for diagenesis of bulk marine carbonate. *Geochim Cosmochim Acta* 59(11):2265–2278.
16. Schrag DP (1999) Effects of diagenesis on the isotopic record of late Paleogene tropical sea surface temperatures. *Chem Geol* 161(1–3):215–224.
17. Evans D, Müller W (2012) Deep time foraminifera Mg/Ca paleothermometry : Nonlinear correction for secular change in seawater Mg/Ca. *Paleoceanography* 27:1–11.
18. Tierney JE, Tingley MP (2014) A Bayesian, spatially-varying calibration model for the TEX<sub>86</sub> proxy. *Geochim Cosmochim Acta* 127:83–106.
19. Ho SL, Laepple T (2016) Flat meridional temperature gradient in the early Eocene in the subsurface rather than surface ocean. *Nat Geosci* 9:606–610.
20. Hollis CJ, et al. (2012) Early Paleogene temperature history of the Southwest Pacific Ocean : Reconciling proxies and models. *Earth Planet Sci Lett* 349–350:53–66.
21. Evans D, Wade BS, Henahan M, Erez J, Müller W (2016) Revisiting carbonate chemistry controls on planktic foraminifera Mg/Ca: Implications for sea surface temperature and hydrology shifts over the Paleocene-Eocene Thermal Maximum and Eocene-Oligocene transition. *Clim Past* 12(4):819–835.
22. Boucher O, Randall D (2013) Clouds and Aerosols. *Climate Change 2013: The Physical Science Basis*. pp 571–657.
23. Huber M (2008) Climate change. A hotter greenhouse? *Science* 321(5887):353–4.
24. Williams IN, Pierrehumbert RT, Huber M (2009) Global warming, convective threshold and false thermostats. *Geophys Res Lett* 36(21):2–6.
25. Spicer RA, et al. (2014) Cool tropics in the Middle Eocene: Evidence from the Changchang Flora, Hainan Island, China. *Palaogeogr Palaoclimatol Palaeoecol* 412:1–16.
26. Ghosh P, et al. (2006) <sup>13</sup>C–<sup>18</sup>O bonds in carbonate minerals: A new kind of paleothermometer. *Geochim Cosmochim Acta* 70(6):1439–1456.
27. Zaarur S, Affek HP, Brandon MT (2013) A revised calibration of the clumped isotope thermometer. *Earth Planet Sci Lett* 382:47–57.
28. Tang J, Dietzel M, Fernandez A, Tripati AK, Rosenheim BE (2014) Evaluation of kinetic effects on clumped isotope fractionation (Δ<sub>47</sub>) during inorganic calcite precipitation. *Geochim Cosmochim Acta* 134:120–136.
29. Renema W (2006) Large benthic foraminifera from the deep photic zone of a mixed siliciclastic-carbonate shelf off East Kalimantan, Indonesia. *Mar Micropaleontol* 58(2):73–82.
30. Evans D, Müller W, Oron S, Renema W (2013) Eocene seasonality and seawater alkaline earth reconstruction using shallow-dwelling large benthic foraminifera. *Earth Planet Sci Lett* 381:104–115.
31. Inglis GN, et al. (2015) Descent toward the Icehouse: Eocene sea surface cooling inferred from GDGT distributions. *Paleoceanography* 30(7):1000–1020.
32. Kozdon R, Kelly DC, Kita NT, Fournelle JH, Valley JW (2011) Planktonic foraminiferal oxygen isotope analysis by ion microprobe technique suggests warm tropical sea surface temperatures during the Early Paleogene. *Paleoceanography* 26.
33. Coggon RM, Teagle D a H, Smith-Duque CE, Alt JC, Cooper MJ (2010) Reconstructing

**Acknowledgments:** We thank the editor, and reviewers for their constructive comments which greatly improved this contribution. DE and HPA acknowledge support from Yale University and the Yale Analytical and Stable Isotope Center and from grant 171116 of the Israel Science Foundation. WR and LJC were supported by NWO grant number ALW 822 01 009. COSTECH and the Tanzania Petroleum Development Corporation supported the TDP which recovered the Tanzanian specimens. LA-ICPMS work at RHUL was partly funded by a 2014 NERC Capital Equipment Grant (Ref: CC073). The Research Foundation Flanders (FWO) is acknowledged for financial support to PS. MZ acknowledges support from the Netherlands Earth System Science Center (NESSC) and Horizon 2020 grant MSCA-IF-2014 655073.

- past seawater Mg/Ca and Sr/Ca from mid-ocean ridge flank calcium carbonate veins. *Science* 327(5969):1114–7.
34. Gothmann AM, et al. (2015) Fossil corals as an archive of secular variations in seawater chemistry since the Mesozoic. *Geochim Cosmochim Acta* 160:188–208.
35. Stanley SM, Hardie LA (1998) Secular oscillations in the carbonate mineralogy of reef-building and sediment-producing organisms driven by tectonically forced shifts in seawater chemistry. *Palaogeogr Palaoclimatol Palaeoecol* 144:3–19.
36. Wilkinson B, Algeo T (1989) Sedimentary carbonate record of calcium-magnesium cycling. *Am J Sci* 289:1158–1194.
37. Evans D, Erez J, Oron S, Müller W (2015) Mg/Ca-temperature and seawater-test chemistry relationships in the shallow-dwelling large benthic foraminifera Operculina ammonoides. *Geochim Cosmochim Acta* 148:325–342.
38. Hönisch B, et al. (2013) The influence of salinity on Mg/Ca in planktic foraminifers – Evidence from cultures, core-top sediments and complementary δ<sup>18</sup>O. *Geochim Cosmochim Acta* 121:196–213.
39. Hay WW, et al. (2006) Evaporites and the salinity of the ocean during the Phanerozoic: Implications for climate, ocean circulation and life. *Palaogeogr Palaoclimatol Palaeoecol* 240(1–2):3–46.
40. Tierney JE, Sinninghe Damsté JS, Pancost RD, Sluijs A, Zachos JC (2017) Eocene temperature gradients. *Nat Geosci* 10(8):538–539.
41. Tripati AK (2003) Tropical sea-surface temperature reconstruction for the early Paleogene using Mg/Ca ratios of planktonic foraminifera. *Paleoceanography* 18(4). doi:10.1029/2003PA000937.
42. Sluijs A, et al. (2008) Arctic late Paleocene–early Eocene paleoenvironments with special emphasis on the Paleocene-Eocene thermal maximum (Lomonosov Ridge, Integrated Ocean Drilling Program Expedition 302). *Paleoceanography* 23(1):1–17.
43. Bijl PK, et al. (2013) Eocene cooling linked to early flow across the Tasmanian Gateway. *Proc Natl Acad Sci* 110(24):9645–9650.
44. Cramer BS, Miller KG, Barrett PJ, Wright JD (2011) Late Cretaceous–Neogene trends in deep ocean temperature and continental ice volume: Reconciling records of benthic foraminiferal geochemistry (δ<sup>18</sup>O and Mg/Ca) with sea level history. *J Geophys Res* 116:1–23.
45. Douglas PMJ, et al. (2014) Pronounced zonal heterogeneity in Eocene southern high-latitude sea surface temperatures. *Proc Natl Acad Sci* 111(18):6582–7.
46. Sagoo N, Valdes P, Flecker R, Gregoire LJ (2013) The Early Eocene equable climate problem: can perturbations of climate model parameters identify possible solutions? *Philos Trans R Soc A Math Phys Eng Sci* 371:20130123.
47. Lunt DJ, et al. (2010) CO<sub>2</sub>-driven ocean circulation changes as an amplifier of Paleocene-Eocene thermal maximum hydrate destabilization. *Geology* 38(10):875–878.
48. Roberts CD, LeGrande AN, Tripati AK (2009) Climate sensitivity to Arctic seaway restriction during the early Paleogene. *Earth Planet Sci Lett* 286(3–4):576–585.
49. Huber M, Caballero R (2011) The early Eocene equable climate problem revisited. *Clim Past* 7(2):603–633.
50. Winguth A, Shellito C, Shields C, Winguth C (2010) Climate response at the paleocene-eocene thermal maximum to greenhouse gas forcing-a model study with CCSM3. *J Clim* 23(10):2562–2584.
51. Schneider T, et al. (2017) Climate goals and computing the future of clouds. *Nat Clim Chang* 7(1):3–5.
52. Hay WW, et al. (1999) Alternative global Cretaceous paleogeography. *Evolution of the Cretaceous Ocean-Climate System*, eds Barrera E, Johnson CC (Geological Society of America Special Publication), pp 1–39.
53. Horita J, Zimmermann H, Holland HD (2002) Chemical evolution of seawater during the Phanerozoic. *Geochim Cosmochim Acta* 66(21):3733–3756.
54. Evans D, Brierley C, Raymo ME, Erez J, Müller W (2016) Planktic foraminifera shell chemistry response to seawater chemistry: Pliocene-Pleistocene seawater Mg/Ca, temperature and sea level change. *Earth Planet Sci Lett* 438:139–148.
55. Higgins JA, Schrag DP (2015) The Mg isotopic composition of Cenozoic seawater - evidence for a link between Mg-clays, seawater Mg/Ca, and climate. *Earth Planet Sci Lett* 416:73–81.
56. Kim J-H, et al. (2010) New indices and calibrations derived from the distribution of renaissance isoprenoid tetraether lipids: Implications for past sea surface temperature reconstructions. *Geochim Cosmochim Acta* 74(16):4639–4654.
57. Heinemann M, Jungclauss JH, Marotzke J (2009) Warm Paleocene/Eocene climate as simulated in ECHAM5/MPI-OM. *Clim Past* (1987):785–802.
58. Müller W, Shelley M, Miller P, Broude S (2009) Initial performance metrics of a new custom-designed ArF excimer LA-ICPMS system coupled to a two-volume laser-ablation cell. *J Anal At Spectrom* 24(2):209.
59. Zaarur S, Affek HP, Stein M (2016) Last glacial-Holocene temperatures and hydrology of the Sea of Galilee and Hula Valley from clumped isotopes in Melanopsis shells. *Geochim Cosmochim Acta* 179:142–155.
60. Dennis KJ, Affek HP, Passy BH, Schrag DP, Eiler JM (2011) Defining an absolute reference frame for “clumped” isotope studies of CO<sub>2</sub>. *Geochim Cosmochim Acta* 75(22):7117–7131.

749  
750  
751  
752  
753  
754  
755  
756  
757  
758  
759  
760  
761  
762  
763  
764  
765  
766  
767  
768  
769  
770  
771  
772  
773  
774  
775  
776  
777  
778  
779  
780  
781  
782  
783  
784  
785  
786  
787  
788  
789  
790  
791  
792  
793  
794  
795  
796  
797  
798  
799  
800  
801  
802  
803  
804  
805  
806  
807  
808  
809  
810  
811  
812  
813  
814  
815  
816